Manuscript
Click here to view linked References

Submitted to Materials Science and Engineering A (Revised: August 2017)

Microstructure and properties of a CoCrFeNiMn high-entropy alloy processed by equal-channel angular pressing

Hamed Shahmir[a], Tayebeh Mousavi[b], Junyang He[c], Zhaoping Lu[c], Megumi Kawasaki[d], Terence G. Langdon[a,*]

[a] *Materials Research Group, Faculty of Engineering and the Environment, University of Southampton, Southampton SO17 1BJ, UK*
[b] *Department of Materials, University of Oxford, Parks Road, Oxford OX1 3PH, UK*
[c] *State Key Laboratory for Advanced Metals and Materials, University of Science and Technology Beijing, Beijing 10083, People's Republic of China*
[d] *Division of Materials Science and Engineering and the Research Institute of Industrial Science, Hanyang University, Seoul 133-791, South Korea*

Abstract

A CoCrFeNiMn high-entropy alloy (HEA) was processed by equal-channel angular pressing (ECAP) for up to four passes at 673 K and the results show that the strength increases gradually with increasing straining up to ~1 GPa with an elongation to failure of ~35% after four passes of ECAP. In this condition, the microstructure is a single-phase ultrafine-grained (UFG) CoCrFeNiMn HEA with an average grain size of ~100 nm and a high dislocation density. This UFG HEA was subjected to post-deformation annealing (PDA) at temperatures of 673-1073 K for 60 min and it is shown that the hardness increases slightly due to precipitation to 773 K and then decreases to 1073 K due to a combination of recrystallization, grain growth and a dissolution of precipitates. The formation of brittle σ-phase precipitates improves the strength significantly but with a minor decrease in ductility. Annealing at the peak temperature of 773 K produces a very high yield strength of ~1015 MPa and an ultimate strength of ~1080 MPa together with an excellent elongation to failure of ~30%. An analysis of the data shows that grain boundary strengthening is the most important strengthening mechanism in these ECAP samples both before and after PDA.

Keywords: CoCrFeNiMn; High-entropy alloy; Equal-channel angular pressing; Post-deformation annealing; Severe plastic deformation.

*Corresponding author. Tel.: +442380593766; e-mail address: langdon@soton.ac.uk

1. Introduction

The equiatomic CoCrFeNiMn alloy is a single-phase *fcc* solid solution high-entropy alloy (HEA) having high strength and high ductility [1-3]. This alloy generally exhibits good mechanical properties including outstanding ductility at liquid nitrogen temperature [2,4] and a room temperature yield strength and ductility around ~300 MPa and ~85% in the homogenized condition [5]. In order to increase the strength without significantly sacrificing the ductility, additional strengthening methods may be needed. Thus, it was shown that thermo-mechanical processing, including cold rolling followed by annealing, enhanced the yield strength of the alloy by refining the grains from ~144 to ~4.4 μm [6] and this suggested grain boundary hardening may be useful although the degree of hardening was not exceptional. Accordingly, it is reasonable to anticipate that further grain refinement using severe plastic deformation (SPD) methods may lead to additional strengthening of the alloy.

It is well known that grain refinement by SPD can improve the physical and mechanical properties of metals and alloys [7-9]. For example, it was shown for the CoCrFeNiMn alloy that processing by the SPD technique of high-pressure torsion (HPT) leads to exceptional grain refinement to ~10 nm and a significant increase in strength to ~1.75 GPa, a hardness of ~4.41 GPa and a very low ductility of ~4% at room temperature [5]. The high strength but limited ductility of nanostructured alloys processed by HPT is due to their low rate of strain hardening and low strain rate sensitivity [10,11]. For this reason, post-deformation annealing (PDA) of the nanostructured alloys is often important for improving the overall ductility. In practice, however, the use of PDA in this alloy is challenging because of the decomposition and formation of new phases in the *fcc*-matrix in the range of 673-1073 K [12-16]. For example, it was shown that the formation of brittle precipitates, especially the σ-phase, at 873 and 973 K, significantly reduced the ductility of the HPT-processed alloy whereas short-term annealing for 10 min at 1073 K prevented grain growth and gave a combination of high strength and good

ductility including an ultimate tensile strength of ~830 MPa and an elongation to failure of ~65% [5].

Processing by equal-channel angular pressing (ECAP) [17] is generally considered superior to most other SPD techniques because it uses relatively large bulk samples, it can be combined with appropriate thermo-mechanical treatments to produce long rods [18] and it has a general simplicity in operation [19]. Thus, selecting an appropriate processing condition may provide the potential for producing both good ductility and high strength in selected HEAs. A review of the literature shows that ECAP was used for powder consolidation of HEA [20] but there are no reports to date of the application of ECAP to bulk solids and there are no reports describing the influence of ECAP processing on the microstructural evolution or the mechanical characteristics of any HEAs. Accordingly, the present research was initiated to evaluate the effect of ECAP and subsequent PDA on microstructural development and the mechanical properties of a CoCrFeNiMn HEA.

2. Experimental material and procedures

The experiments were conducted on an HEA with a nominal composition of $Co_{20}Cr_{20}Fe_{20}Ni_{20}Mn_{20}$ (in at.%) where the alloy was prepared by arc-melting a mixture of pure metals (purity >99 wt.%). The ingot was remelted at least four times to promote chemical homogeneity and then the melted alloy was drop-cast into a mould to give a bar of about 10 × 10 mm^2 with a length of ~60 mm. The as-cast alloy was hot-forged at 1373 K and then homogenized at 1473 K for 12 h under a controlled atmosphere. The grain size after homogenization was ~100 μm. Billets with lengths of ~60 mm and diameters of 10 mm were prepared by machining. All billets were processed by ECAP at 673 K using a solid die with an internal channel angle, φ, of 110° where it can be shown that this value of φ produces an equivalent strain, ε_{eq}, of ~0.8 on each separate pass through the die [21]. Billets were processed for up to four passes of ECAP to give a maximum equivalent strain of ~3.2 and the pressing was conducted using route B_C in which each sample is rotated by 90° in the same sense

between consecutive passes [22]. The pressing rate was maintained at 3 mm s^{-1} and molybdenum disulphide (MoS_2) was used as a lubricant. The samples processed through four ECAP passes were used for PDA at temperatures of 673-1073 K for 60 min.

Measurements of the Vickers microhardness, Hv, were taken at the centres of the longitudinal sections of the billets parallel to the pressing direction, where this is equivalent to the *X* direction in the conventional depiction of ECAP [17]. For the microhardness measurements, a load of 500 gf was applied for a dwell time of 10 s and every point in the values reported for Hv represents the average of five separate hardness values. The phase constituents were determined using X-ray diffraction (XRD) employing Cu Kα radiation (wavelength $\lambda = 0.154$ nm) at 45 kV and a tube current of 200 mA. The XRD measurements were performed over a 2θ range from 30° to 100° using a scanning step of 0.02° and a scanning speed of 2° min^{-1}.

Microstructural characterizations were carried out with scanning electron microscopy (SEM) using a JSM6500F thermal field emission microscope and transmission electron microscopy (TEM) using a JEOL JEM-3010 microscope operating under an accelerating voltage of 300 kV. For SEM observations in the secondary imaging mode, the samples were ground through 800, 1200 and 4000-grit SiC paper and then polished using a 40 nm colloidal silica suspension. Foils for the TEM observations were prepared using a focused ion beam (FIB) (Zeiss Nvision 40 FIB) facility at the cross-section of the centre of the billet after the fourth pass of ECAP and after PDA at 773 K for 60 min, with the observations performed on the normal to the pressing direction so that the normal of the image lies in the *X* direction. For the initial bulk milling a 30 kV Ga beam was used, but the final milling step was performed using a 2 kV accelerating voltage and a 200 pA current in order to limit the penetration of Ga^+ ions into the sample.

Two tensile specimens were cut from the longitudinal sections of the billets parallel to the pressing direction using electro-discharge machining with the specimens having gauge

dimensions of 4.0 × 3.0 × 2.0 mm^3. The mechanical properties were examined at room temperature in the initial condition before and after ECAP and after PDA at 773-973 K for 60 min. Two samples were tested for each condition. Stress-strain curves were recorded with a Zwick universal testing machine operating at a constant rate of cross-head displacement with an initial strain rate of ~1.0×10^{-3} s^{-1}

3. Experimental results

3.1 Microstructure after ECAP processing

Figure 1 shows X-ray diffraction patterns of the homogenized unprocessed sample (labeled 0p) and longitudinal sections of the processed HEA after one, two and four passes (1p, 2p and 4p, respectively). The results demonstrate that the initial and ECAP-processed microstructures consist of a single *fcc* phase and ECAP processing at 673 K does not lead to the formation of any precipitates. Figure 1 also illustrates the effect of the ECAP processing on peak broadening in the HEA where this broadening in the solution annealed condition denotes energy storage during ECAP processing. This broadening may be used to estimate the grain size and dislocation density in the ECAP-processed HEA using the classical Williamson-Hall method and the following simple equation can be used for estimating the dislocation density [23,24]:

$$\rho = \frac{\bar{\varepsilon}}{} \qquad (1)$$

where ρ, b and ε are dislocation density, Burgers vector and microstrain, respectively. Considering a Burgers vector of b = 0.255 nm [25], processing through four ECAP passes gave an estimated grain size of $d \approx 100$ nm, a microstrain of ~0.0001 and a dislocation density of $\rho \approx 1.3 \times 10^9$ cm^{-2}. Table 1 summarizes the estimated values obtained after processing by ECAP through one, two and four passes.

Representative TEM micrographs and a selected area electron diffraction (SAED) pattern are shown in Fig. 2 at the cross-sections of the billets after four passes of ECAP. It is readily apparent that in the processed state the microstructure is highly strained with complicated non-uniform contrasts because of the presence of high densities of lattice defects. Careful

observations showed that many of the grains had irregular shapes and they were often surrounded by boundaries that were wavy and not well delineated. The images indicated an average size for the separate structural fragments of ~100 nm. The diffraction pattern in Fig. 2(a) corresponds to the *fcc* phase with significant streaking of the diffraction spots indicating the presence of high internal stresses and elastic distortions within the crystal lattice. These observations are typical of conventional metals processed using SPD techniques and they demonstrate the presence of a large volume of high-energy non-equilibrium grain boundaries [26-28]. Electron dispersive spectroscopy (EDS) of the region shown in Fig. 2(b) gave a chemical composition which is very close to the nominal composition.

3.2 Mechanical properties after ECAP processing

The values of the Vickers microhardness, Hv, are summarized in Table 1 at the centres on longitudinal sections of the HEA after one, two and four passes. Inspection shows there is a very significant increase in the hardness values with increasing numbers of passes with an initial hardness of Hv ≈ 135 and a final hardness of Hv ≈ 315 after four passes.

Representative plots of engineering stress against engineering strain for the homogenized sample (0p) and after ECAP through one, two and four passes are shown in Fig. 3 for an initial strain rate of 1.0×10^{-3} s^{-1}. The relevant data for the engineering yield stress (YS), ultimate tensile stress (UTS), elongation (δ) and uniform strain of each sample are summarized in Table. 1. Inspection of the curves in Fig. 3 shows there is initially a large elongation to failure and a low flow stress in the unprocessed condition but ECAP processing produces a significant increase in strength with a corresponding decrease in the measured elongations to failure. This is consistent with the classical mechanical behavior of ultra-fine grained (UFG) metals that are tested in tension at relatively low temperatures after processing using SPD techniques [29]. The results show a UTS of ~1 GPa after four passes of ECAP and a corresponding elongation to failure of ~35%. This compares with an initial homogenized strength and elongation to failure of ~500 MPa and ~90%, respectively.

3.3 Microstructure after PDA

Figure 4 shows the measured values of the microhardness of samples processed through 4 passes and after annealing at temperatures of 673 to 1073 K for a period of 60 min with the lower dashed line at Hv ≈ 135 corresponding to the initial hardness in the homogenized condition. The results show that the hardness increases slightly up to Hv ≈ 340 after annealing at 773 K but thereafter it decreases rapidly with increasing annealing temperatures up to 1073 K. Earlier results showed that the homogenized alloy also exhibits a similar trend but with a maximum hardness in the coarse-grained material of only Hv ≈ 200 [5]. This behavior provides strong evidence that precipitates form at temperatures up to 773 K.

Microstructural evaluations of the UFG HEA after PDA were conducted using XRD and the results are given in Fig. 5. Close inspection shows the presence of some additional peaks of very low intensities, marked with open squares in Fig. 5, in the samples annealed at temperatures in the range of 773 to 973 K. The crystal structure of this new phase was identified as tetragonal with lattice parameters of $a \approx 8.8$ Å and $c \approx 4.5$ Å. This is consistent with the σ-phase which is a hard Cr-rich phase reported earlier in HEAs [5,12,14,15]. Nevertheless, the XRD results in Fig. 5 indicate that the microstructure reverts again to a single phase after annealing at 1073 K.

A set of representative TEM images, an appropriate SAED pattern and an EDS analysis are shown in Fig. 6 for the sample processed through 4 passes of ECAP followed by PDA at the critical temperature of 773 K for 60 min. The images at different magnifications in Figs 6(a,b) show that PDA at this temperature leads to a highly strained microstructure with complicated non-uniform contrasts associated with the high density of lattice defects. The TEM image with corresponding SAED pattern shown in Figs. 6(c) and (d) demonstrates the formation of precipitates in the microstructure. The width of these precipitates is ~60 nm. New spots corresponding to these σ-phase precipitates are present in the SAED pattern in Fig. 6(d) and there is also significant streaking of the diffraction spots of the *fcc* phase. Figures 6(e) and (f)

represent higher magnification bright and dark-field TEM images, respectively, of the plate-like precipitate shown in Fig. 6(c). The dark-field image in Fig. 6(f) is based on the spot corresponding to the σ-phase marked by an arrow in the SAED pattern in Fig. 6(d). The EDS analyses of the matrix and precipitate, labelled as A and B, respectively, in Fig. 6(f), confirm that the precipitate corresponds to the σ Cr-rich phase.

Figure 7 shows SEM microstructures (a) after ECAP processing for 4 passes and after PDA for 60 min at (b) 873, (c) 973 and (d) 1073 K. These images provide clear evidence that the microstructure remains essentially unchanged after PDA at 873 K whereas at 973 K there is partial recrystallization and at 1073 K there is full recrystallization with an equiaxed microstructure having an average grain size of ~3 μm. There is also evidence for the occurrence of twinning in Fig. 7(d).

3.4 *Mechanical properties after PDA*

Using an initial strain rate of 1.0×10^{-3} s^{-1}, representative plots of engineering stress against engineering strain are shown in Fig. 8 for samples processed through 4 passes of ECAP and after PDA for 60 min at temperatures of 773, 873 and 973 K. Table 2 summarizes the mechanical properties data and also includes results for similar samples processed through two passes of ECAP and subjected to PDA at the same temperatures. Annealing at 773 K gives a reasonable UTS of ~1080 MPa with an elongation to failure of ~30% without significant strain hardening. However, the strength decreases at higher annealing temperatures although the elongation to failure increases up to 973 K. It is apparent from Table 2 and Fig. 8 that the elongations to failure after PDA at 773 and 873 K are lower than immediately following the ECAP processing. This is attributed to the formation of precipitates in the microstructure during the PDA. It is also apparent from Table 2 that PDA at 973 K leads to a significant improvement in the elongation to failure but with a reduction in the UTS. It is concluded that PDA at 773 and 873 K for 60 min leads to excellent mechanical properties with a UTS >1 GPa after processing by ECAP for four passes and with elongations to failure of at least 30%.

Comparable results were also obtained after processing through two ECAP passes followed by PDA but with lower strengths and higher elongation to failure. After annealing at 973 K the mechanical properties in both conditions were very similar.

4. Discussion

4.1 *Microstructural evolution during ECAP processing*

These microstructural observations reveal an average size of separate fragments of ~100 nm and the formation of a single-phase UFG CoCrFeNiMn HEA after four passes of ECAP. The microstructural evolution in this CoCrFeNiMn alloy during rolling and HPT processing at room temperature was associated with intensive deformation twinning and these twin boundaries play a significant role in the evolution and/or the refinement of the microstructure during further straining following the saturation of twinning [5,30]. An earlier report showed that at a deformation temperature up to 873 K during tensile testing the initial plasticity occurred exclusively by planar glide of 1/2<110> dislocations on {111} planes and at higher strains the slip became more homogeneous with the development of cell structures [2]. The microstructural analyses in the present study show that SPD by ECAP processing of the CoCrFeNiMn HEA at 673 K leads to the formation of a dislocation density of $\rho \approx 1.3 \times 10^{9}$ cm^{-2} after four passes. In addition, the mechanical results reveal significant hardening after ECAP processing. Both the microhardness and the UTS demonstrate incremental improvements of ~100% after four passes of ECAP. Thus, hardening occurs due to the dislocation density and dislocation slip during ECAP processing at 673 K.

An earlier study on the same material suggested that a phase decomposition may take place during annealing at 673 K after HPT processing [5]. In the present study, ECAP processing was conducted at 673 K and the subsequent hardness increment after PDA at higher temperatures is consistent with the occurrence of decomposition at this temperature. Nevertheless, no decomposition was detected in the microstructures after ECAP and this is probably due to the short holding time at 673 K during the ECAP process and the occurrence of

sluggish diffusion in the CoCrFeNiMn HEA which is a well-known and inherent feature of these alloys [31-33].

4.2 *Microstructural evolution during PDA*

The observations show that the initial and the ECAP-processed microstructures consist of a single *fcc* phase. However, the substantial increase in hardness upon annealing combined with the XRD and microstructural evaluations suggest that phase decomposition takes place during PDA at 673-973 K. The hardness exhibits a slight increase to 773 K due to the formation of this new phase and then a subsequent decrease up to 1073 K in Fig. 4 due to a combination of recrystallization and grain growth.

The decomposition and the formation of new phases in the *fcc*-matrix were reported earlier in CoCrFeNiMn HEAs after annealing within special temperature ranges [5,12,14,15]. Furthermore, the XRD results in this study in Fig. 5 confirm the formation of σ Cr-rich precipitates during annealing at 773-973 K and the TEM images and EDS analysis in Fig. 6 after PDA at 773 K also confirm the formation of this σ-phase. It is important to note that the σ-phase was not detected after annealing in the homogenized condition [5,34]. Thus, it appears that the severely-deformed structure of the ECAP-processed HEA facilitates the phase decomposition and this must be due to the large numbers of defects and grain boundaries introduced during ECAP which serve both as fast diffusion pathways and as preferential nucleation sites for the formation of new phases. It is therefore concluded that the occurrence of severe deformation leads more quickly to the formation of these stable phases.

It was also reported earlier that recrystallization occurs after PDA at $T > 973$ K and this is consistent with the dissolution of the precipitates. Generally, the HEA has a high recrystallization temperature and a strong resistance to grain coarsening during annealing [35-37]. Close inspection of the hardness data shows that the hardness decreases significantly above 773 K due to a dissolution of the precipitates and to the activation of the recrystallization mechanism up to 1073 K so that finally, at 1073 K, the hardness is close to the homogenized

condition due to grain growth. The microstructural evolution during PDA, as studied by TEM and SEM, indicates that recrystallization starts above 873 K and finishes at 1073 K as shown in Fig. 7. At this significantly high recrystallization temperature (>973 K), the low rate of grain growth produces excellent stability in the UFG structure and this is attributed to the nature of the distorted matrix which is characterized by a high lattice energy, a sluggish diffusion effect and a low stacking fault energy [35].

4.3 Effect of ECAP and PDA on the mechanical properties

Because of the success in these experiments in achieving a highly-refined microstructure in the HEA by ECAP, it is readily apparent from Fig. 8 that the tensile properties of the ECAP-processed specimens are satisfactory when testing at room temperature. The elongation to failure of 35% after four passes of ECAP demonstrates a reasonable ductility which is generally sufficient for most engineering applications. Furthermore, the results show that the formation of precipitates after PDA at 773-873 K produces a drop in the measured elongations to failure.

It is important to note that the size and geometry of the specimens play a role in determining the results obtained in tensile testing. For example, it was shown that the measured elongations to failure in tensile testing tend to increase with decreasing gauge length [38,39] and this is because the area of necking constitutes a major fraction of the gauge length in samples with very short gauge lengths so that much of the measured elongation in simple tensile testing is related to flow in the necked region. This suggests, therefore, that it may be unreasonable to make a direct comparison between the total elongations achieved in conventional tensile testing with longer gauge lengths with those results obtained in tensile testing using ECAP samples with gauge lengths of the order of ~4 mm. Instead, it appears initially that a more realistic comparison may be achieved by measuring the uniform strain occurring prior to the formation of the neck as reported in Tables 1 and 2. However, it is worthwhile noting that the gauge thicknesses in the ECAP tensile samples are very small, typically of the order of ~2 mm, and this may easily lead to premature failure because there are

insufficient grains in the cross-sectional areas to maintain deformation to very high elongations.

The tensile testing results suggest that the newly-formed phase after PDA has an intermetallic character which provides high strength. The formation of precipitates causes decreasing ductility in the HEA at 773-873 K where the σ-phase is stable but PDA at T > 873 K leads to a significant improvement in the elongation to failure but with a corresponding reduction in strength. It is important to note that the precipitated phases are dissolved at 1073 K and it is reasonable to expect that grain coarsening starts at this temperature. It was suggested earlier that this alloy softens as the grains grow above 1023 K and the strength of the alloy obeys the classical Hall-Petch relationship although the hardening coefficient is then larger than in conventional *fcc* metals [35].

This investigation shows that the processing of the CoCrFeNiMn HEA by a combination of ECAP through four passes and PDA at 773 K for 60 min leads to a very high yield strength of ~1015 MPa, an ultimate tensile strength of ~1080 MPa and a significant elongation to failure of ~30%. Reasonably similar results were also obtained by PDA at 873 K. Nevertheless, PDA at the higher temperature of 973 K leads to an acceleration in recrystallization and grain growth and a consequent reduction in strength.

4.4 The nature of the strengthening mechanisms

A structure-based strength calculation model may be used to estimate the theoretical strength and thereby to provide important information on the nature of the strengthening mechanisms and the correlation between microstructure and yield stress of the HEA after processing by ECAP and PDA.

First, it is assumed that the yield stress, $\sigma_{0.2}$, of the sample is given by a simple summation of the strengthening contributions from individual crystal defects that are acting as obstacles for dislocation slip, so that [40]:

$$\sigma_{0.2} = \sigma_0 + \sigma_{gb} + \sigma_\rho + \sigma_P \quad (2)$$

where σ_0 is the lattice friction strength which is assumed as 165 MPa [41] and σ_{gb}, σ_ρ and σ_P are

the contributions from grain boundary strengthening, dislocation strengthening and precipitation strengthening, respectively. In order to calculate each strengthening contribution after ECAP processing and PDA, several assumptions are needed but it is important to note initially that there are no precipitates in the microstructure after ECAP processing so that σ_P is not included in the strengthening of the ECAP-processed sample.

Tt is known that grain refinement will generally improve the strength of metals and alloys due to introduction of a high volume fraction of grain boundaries which impede dislocation motion. The grain boundary strengthening, σ_{gb}, is described by the classical Hall-Petch relationship [42,43]:

$$\sigma_{gb} = k_y d^{-1/2} \quad (3)$$

where d is the grain size and ky is the strengthening coefficient which is equal to 226 MPa.$\mu m^{1/2}$ for the CoCrFeNiMn system [44]. The TEM and SEM observations in Figs. 2, 6 and 7 give average grain sizes of ~0.10 μm after four pass ECAP and ~0.10 and ~0.12 μm after PDA at 773 and 873 K, respectively. Recrystallization in PDA at 973 K leads to an increase in grain size to ~0.8 μm in Fig. 7(c).

The Bailey-Hirsch relationship may be used for dislocation strengthening so that [45]:

$$\sigma_\rho = M\alpha Gb\rho^{1/2} \quad (4)$$

where M is the Taylor factor (~3.06 [46]), α is a constant (~0.2 [47]), G is the shear modulus (~81 GPa [48]), b is the Burgers vector (0.255 nm [25]) and ρ is the total dislocation density which was calculated from the XRD results in Fig. 5 using the classical Williamson-Hall method [23,24]. This suggests that annealing at temperatures of <973 K is insufficient to annihilate the large numbers of dislocations created during ECAP processing whereas in PDA at temperatures above 973 K the advent of recrystallization leads to an annihilation of ~90% of the dislocations.

The increase in the yield and tensile strengths of the annealed samples after precipitation of the σ-phase is readily evident from the stress-strain plots. The yield strength (YS) increased

from ~980 to ~1015 MPa after PDA at 773 K and it is important to note that there is no corresponding significant change in either the grain size or the dislocation density before and after the PDA at 773 K. Therefore, the experiments show that that there is an improvement in the YS due to second phase precipitation within the *fcc* matrix of ~35 MPa. The Orowan mechanism is generally invoked to explain precipitation strengthening theoretically by hard precipitates using a dislocation by-pass mechanism where this mechanism occurs when the radius of the particles exceeds a critical value or is incoherent with the matrix [49]. Precipitation strengthening by the Orowan mechanism is given by [49]:

$$\sigma_P = \frac{0.8MGb}{\lambda_\sigma} \tag{5}$$

where λ_σ is the average inter-precipitate spacing. Assuming the particles are randomly distributed within the matrix, the value of λ_σ may be calculated from the relationship [50]:

$$\lambda_\sigma = \frac{4(1-f)r}{3f} \tag{6}$$

where f is the volume fraction of the σ precipitates and r is the mean precipitate radius. The volume fractions of these precipitates may be estimated using the XRD results in Fig. 5, giving values of ~4, ~5 and ~6% for samples after PDA at 773, 873 and 973 K, respectively. It is difficult to estimate the mean precipitate radius because the σ precipitates observed in these experiments are plate-like. Nevertheless, the analysis may be simplified by assuming spherical particles [41] and noting that the size of the precipitates is essentially independent of the annealing temperature. Following this approach, the average radius of the σ precipitates was determined from the TEM images in Fig. 6 as $r \approx 30$ nm.

The calculated strengths obtained using Eq. (2) are summarized in Table 3 and documented in Fig. 9 where the experimental values are denoted by the solid circles. Thus, the results for all experimental conditions are in excellent agreement with the values obtained from the calculations. This analysis shows, therefore, that grain boundary strengthening is the most important strengthening mechanism. Furthermore, the precipitation strengthening arising from the σ precipitates that are present in the samples after PDA may be explained directly through

application of the Orowan mechanism.

5. Summery and conclusion

1- This research was initiated to evaluate the effect of ECAP and post-deformation annealing on the microstructural evolution and mechanical properties of a CoCrFeNiMn HEA. The HEA was successfully processed by ECAP at 673 K for up to four passes and the processed samples were subjected to post-deformation annealing at 673-1073 K for 60 min.

2- The Vickers microhardness of the HEA increased gradually from ~135 to ~315 by increasing the numbers of ECAP passes. The yield stress and ultimate tensile strength reached ~980 and ~990 MPa, respectively, with an acceptable elongation to failure of ~35% for the sample processed through four passes. The microstructure after processing through four passes showed a single-phase ultrafine-grained CoCrFeNiMn HEA with an average grain size of ~100 nm and a high dislocation density of ~1.3×10^{9} cm^{-2}.

3- Post-deformation annealing leads to a higher hardness of ~330 at 773 K due to precipitation of the σ-phase and then to a decrease in hardness up to 1073 K due to a combination of recrystallization, grain growth and the dissolution of precipitates. Annealing below 973 K is beneficial because it improves the strength through the formation of the σ-phase with only a minor deterioration in the ductility. However, annealing at 973 K leads to an acceleration in recrystallization and grain growth and thereby to a reduction in strength. Annealing at 773 K is the optimum condition because it leads to a high yield strength of ~1015 MPa, a high ultimate tensile strength of ~1080 MPa and a reasonable elongation to failure of ~30%).

4- There is good agreement between the measured experimental yield stresses and the calculated values for the CoCrFeNiMn HEA after ECAP processing and after PDA at temperatures from 773 to 973 K. The calculations show that the additional strengthening comes primarily from the grain boundaries through the Hall-Petch relationship.

Acknowledgments

This work was supported in part by the National Natural Science Foundation of China (No. 51531001) (JYH and ZPL), in part by the NRF Korea funded by MoE (No. NRF-2016R1A6A1A03013422) and by MSIP (No. NRF-2016K1A4A3914691) (MK) and in part by the European Research Council under Grant Agreement No. 267464-SPDMETALS (HS and TGL).

References

1. B. Cantor, I.T.H. Chang, P. Knight, A.J.B. Vincent, Microstructural development in equiatomic multicomponent alloys, Mater. Sci. Eng. A 375-377 (2004) 213-218.
2. F. Otto, A. Dlouhý, Ch. Somsen, H. Bei, G. Eggeler, E.P. George, The influences of temperature and microstructure on the tensile properties of a CoCrFeMnNi high-entropy alloy, Acta Mater. 61 (2013) 5743-5755.
3. F. Otto, Y. Yang, H. Bei, E.P. George, Relative effects of enthalpy and entropy on the phase stability of equiatomic high-entropy alloys, Acta Mater. 61 (2013) 2628-2638.
4. B. Gludovatz, A. Hohenwarter, D. Catoor, E.H. Chang, E.P. George, R.O. Ritchie, A fracture-resistant high-entropy alloy for cryogenic applications, Science 345 (2014) 1153-1158.
5. H. Shahmir, J.Y. He, Z.P. Lu, M. Kawasaki, T.G. Langdon, Effect of annealing on mechanical properties of a nanocrystalline CoCrFeNiMn high-entropy alloy processed by high-pressure torsion, Mater. Sci. Eng. A676 (2016) 294.
6. F. Otto, N.L. Hanold, E.P. George, Microstructural evolution after thermomechanical processing in an equiatomic, single-phase CoCrFeMnNi high-entropy alloy with special focus on twin boundaries, Intermetallics 54 (2014) 39-48.
7. R. Valiev, Materials science: Nanomaterial advantage, Nature 419 (2002) 887-889.
8. R. Valiev, Nanostructuring of metals by severe plastic deformation for advanced properties, Nat. Mater. 3 (2004) 511-516.
9. R.Z. Valiev, Y. Estrin, Z. Horita, T.G. Langdon, M.J. Zehetbauer, Y.T. Zhu, Fundamentals of superior properties in bulk nanoSPD materials, Mater. Res. Lett. 4 (2016) 1-21.
10. R.Z. Valiev, R.K. Islamgaliev, I.V. Alexandrov, Bulk nanostructured materials from severe plastic deformation, Prog. Mater. Sci. 45(2000) 103-189.
11. R.Z. Valiev, A.V. Sergueeva, A.K. Mukherjee, The effect of annealing on tensile deformation behaviour of nanostructured SPD titanium, Scr. Mater. 49 (2003) 669-674.

12. F. Zhang, C. Zhang, S.L. Chen, J. Zhu, W.S. Cao, U.R. Kattner, An understanding of high entropy alloys from phase diagram calculations, CALPHAD 45 (2014) 1-10.
13. B. Schuh, F. Mendez-Martin, B. Völker, E.P. George, H. Clemens, R. Pippan, A. Hohenwarter, Mechanical properties, microstructure and thermal stability of a nanocrystalline CoCrFeMnNi high-entropy alloy after severe plastic deformation, Acta Mater. 96 (2015) 258-268.
14. F. Otto, A. Dlouhý, K.G. Pradeep, M. Kuběnová, D. Raabe, G. Eggeler, E.P. George, Decomposition of the single-phase high-entropy alloy CrMnFeCoNi after prolonged anneals at intermediate temperatures, Acta Mater. 112 (2016) 40-52.
15. E.J. Pickering, R. Muñoz-Moreno, H.J. Stone, N.G. Jones, Precipitation in the equiatomic high-entropy alloy CrMnFeCoNi, Scr. Mater. 113 (2016) 106-109.
16. V. Maier-Kiener, B. Schuh, E. P. George, H. Clemens, A. Hohenwarter, Nanoindentation testing as a powerful scanning tool for assessing phase stability of nanocrystalline high-entropy alloys, Mater. Des. 115 (2017) 479-485.
17. R.Z. Valiev, T.G. Langdon, Principles of equal-channel angular pressing as a processing tool for grain refinement, Prog. Mater. Sci. 51 (2006) 881-981.
18. R.Z. Valiev, T.G. Langdon, Achieving exceptional grain refinement through severe plastic deformation: new approaches for improving the processing technology, Metall. Mater. Trans. A 42A (2011) 2942-2951.
19. T.G. Langdon, Twenty-five years of ultrafine-grained materials: Achieving exceptional properties through grain refinement, Acta Mater. 61 (2013) 7035-7059.
20. V.H. Hammond, M. A. Atwater, K.A. Darling, H.Q. Nguyen, L.J. Kecskes, Equal-channel angular extrusion of a low-density high-entropy alloy produced by high-energy cryogenic mechanical alloying, JOM 66 (2014) 2021-2029.
21. Y. Iwahashi, J. Wang, Z. Horita, M. Nemoto, T.G. Langdon, Principle of equal-channel angular pressing for the processing of ultra-fine grained materials, Scr. Mater. 35 (1996)

143-146.

22. M. Furukawa, Y. Iwahashi, Z. Horita, M. Nemoto, T.G. Langdon, The shearing characteristics associated with equal-channel angular pressing, Mater. Sci. Eng. A 257 (1998) 328-332.
23. G.K. Williamson, W.H. Hall, X-ray line broadening from filed aluminium and wolframOriginal Research, Acta Metall. 1 (1953) 22-31.
24. G.K. Williamson, R.E. Smallman, Dislocation densities in some annealed and cold-worked metals from measurements on the X-ray debye-scherrer spectrum, Phil. Mag. 1 (1956) 34-45.
25. G. Laplanche, P. Gadaud, O. Horst, F. Otto, G. Eggeler, E.P. George, Temperature dependencies of the elastic moduli and thermal expansion coefficient of an equiatomic, single-phase CoCrFeMnNi high-entropy alloy, J. Alloys Compd. 623 (2015) 348.
26. J. Wang, Z. Horita, M. Furukawa, M. Nemoto, N.K. Tsenev, R.Z. Valiev, Y. Ma, T.G. Langdon, An investigation of ductility and microstructural evolution in an Al-3% Mg alloy with submicron grain size, J. Mater. Res. 8 (1993) 2810-2818.
27. M. Furukawa, Z. Horita, M. Nemoto, R.Z. Valiev, T.G. Langdon, Microhardness measurements and the Hall-Petch relationship in an Al-Mg alloy with submicrometer grain size, Acta Mater. 44 (1996) 4619-4629.
28. Y.T. Zhu, J.Y. Huang, J. Gubicza, T. Ungár, Y.M. Wang, E. Ma, R.Z. Valiev, Nanostructures in Ti processed by severe plastic deformation, J. Mater. Res. 18(8) (2003) 1908-1917.
29. R.Z. Valiev, I.V. Alexandrov, Y.T. Zhu, T.C. Lowe, Paradox of strength and ductility in metals processed by severe plastic deformation, J. Mater. Res. 17 (2002) 5-8.
30. N. Stepanov, M. Tikhonovsky, N. Yurchenko, D. Zyabkin, M. Klimova, S. Zherebtsov, A. Efimov, G. Salishchev, Effect of cryo-deformation on structure and properties of CoCrFeNiMn high-entropy alloy, Intermetallics 59 (2015) 8-17.

31. K.Y. Tsai, M.H. Tsai, J.W. Yeh, Sluggish diffusion in Co–Cr–Fe–Mn–Ni high-entropy alloys, Acta Mater. 61 (2013) 4887-4897.
32. S.Y. Chang, C.E. Li, Y.C. Huang, H.F. Hsu, J.W. Yeh, S.J. Lin, Structural and thermodynamic factors of suppressed interdiffusion kinetics in multi-component high-entropy materials, Sci. Reports 4 (2014) 4162.
33. Y. Zhang, T.T. Zuo, Z. Tang, M.C. Gao, K.A. Dahmen, P.K. Liaw, Z.P. Lu, Microstructures and properties of high-entropy alloys, Prog. Mater. Sci. 61 (2014) 1-93.
34. F. He, Z. Wang, Q. Wu, J. Li, J. Wang, C.T. Liu, Phase separation of metastable CoCrFeNi high entropy alloy at intermediate temperatures, Scr. Mater. 126 (2017) 15-19.
35. W.H. Liu, Y. Wu, J.Y. He, T.G. Nieh, Z.P. Lu, Grain growth and the Hall-Petch relationship in a high-entropy FeCrNiCoMn alloy, Scr Mater 68 (2013) 526-529.
36. P.P. Bhattacharjee, G.D. Sathiaraj, M. Zaid, J.R. Gatti, Chi Lee, Che-Wei Tsai, Jien-Wei Yeh, Microstructure and texture evolution during annealing of equiatomic CoCrFeMnNi high-entropy alloy, J. Alloys Compd. 587 (2014) 544-552.
37. G. Dan Sathiaraj, P.P. Bhattacharjee, Analysis of microstructure and microtexture during grain growth in low stacking fault energy equiatomic CoCrFeMnNi high entropy and Ni-60 wt.%Co alloys, J. Alloys Compd. 637 (2015) 267-276.
38. Y.H. Zhao, Y.Z. Guo, Q. Wei, A.M. Dangelewicz, C. Xu, Y.T. Zhu, T.G. Langdon, Y.Z. Zhou, E.J. Lavernia, Influence of specimen dimensions on the tensile behavior of ultrafine-grained Cu, Scr. Mater. 59 (2008) 627-630.
39. Y.H. Zhao, Y.Z. Guo, Q. Wei, T.D. Topping, A.M. Dangelewicz, Y.T. Zhu, T.G. Langdon, E.J. Lavernia, Influence of specimen dimensions and strain measurement methods on tensile stress-strain curves, Mater. Sci. Eng. A 525 (2009) 68-77.
40. N. Kamikawa, K. Sato, G. Miyamoto, M. Murayama, N. Sekido, K. Tsuzaki, T. Furuhara, Stress-strain behavior of ferrite and bainite with nanoprecipitation in low carbon steels, Acta Mater 83 (2015) 383-396.

41. J.Y. He, H. Wang, H.L. Huang, X.D. Xu, M.W. Chen, Y. Wu, X.J. Liu, T.G. Nieh, K. An, Z.P. Lu, A precipitation-hardened high-entropy alloy with outstanding tensile properties, Acta Materialia 102 (2016) 187-196.
42. E.O. Hall, The deformation and ageing of mild steel. III Discussion of results, Proc. Phys. Soc. B 64 (1951) 747-753.
43. N.J. Petch, The cleavage strength of polycrystals, J. Iron Steel Inst. 174 (1953) 25-28.
44. W.H. Liu, Y. Wu, J.Y. He, T.G. Nieh, Z.P. Lu, Grain growth and the Hall-Petch relationship in a high-entropy FeCrNiCoMn alloy, Scr. Mater 68 (2013) 526-529.
45. J.E. Bailey, P.B. Hirsch, The dislocation density, flow stress, and stored energy in cold-worked polycrystalline silver, Phil. Mag. 5 (1960) 485-497.
46. D.A. Hughes, N. Hansen, Microstructure and strength of nickel at large strains, Acta Mater. 48 (2000) 2985-3004.
47. J.Y. He, C. Zhu, D.Q. Zhou, W.H. Liu, T.G. Nieh, Z.P. Lu, Steady state flow of the FeCoNiCrMn high entropy alloy at elevated temperatures, Intermetal. 55 (2014) 9-14.
48. G. Laplanche, P. Gadaud, O. Horst, F. Otto, G. Eggeler, E.P. George, Temperature dependencies of the elastic moduli and thermal expansion coefficient of an equiatomic, single-phase CoCrFeMnNi high-entropy alloy, J. Alloys Compd. 623 (2015) 348-353.
49. E. Orowan, in: M. Cohen (ed.), Dislocations in Metals, AIME, New York, 1954, p. 69.
50. C.W. Corti, P. Cotterill, G. Fitzpatrick, The evaluation of the interparticle spacing in dispersion alloys, Intl Metall. Rev. 19 (1974) 77-88.

Table captions

Table 1. The grain size,d, dislocation density,ρ, Vickers microhardness, YS, UTS, elongation to failure (δ) and uniform strain, of the CoCrFeNiMn HEA before and after ECAP processing at 673 K through different numbers of passes.

Table 2. The Vickers microhardness, YS, UTS, elongation to failure (δ) and uniform strain, of the CoCrFeNiMn HEA before and after post-deformation annealing.

Table 3. The contributions of intrinsic strength (σ_0), grain boundary strengthening (σ_{gb}), dislocation strengthening (σ_ρ) and precipitation strengthening (σ_P) for each condition and comparison between the calculated and experimentally obtained yield stress of an ECAP-processed sample and samples after PDA at 773, 873 and 973 K for 60 min.

Figure captions

Fig. 1 X-ray patterns of the homogenized (0p) condition and samples processed through one to four passes of ECAP.

Fig. 2 (a) TEM image and corresponding SAED pattern of transverse section of a CoCrFeNiMn billet processed by ECAP through four passes at 673 K and (b) TEM image with higher magnification and chemical composition after EDS analysis.

Fig. 3 Stress-strain curves at an initial strain rate of 1.0×10^{-3} s^{-1} in the initial annealed condition (0p) and after ECAP processing through one to four passes.

Fig. 4 Dependence of Vickers hardness of the ECAP-processed samples on the annealing temperature when annealing for 60 min: the lower dashed line shows the homogenized initial condition.

Fig. 5 X-ray patterns after four passes of ECAP followed by PDA at 673 to 1073 K for 60 min.

Fig. 6 TEM images of transverse sections of a CoCrFeNiMn HEA processed by ECAP through four passes at 673 K followed by PDA at 773 K for 60 min: (a-c) grains with mean grain size of ~500 nm, (d) corresponding SAED pattern from the area in (c) containing precipitates, (e) bright and (f) dark-field TEM images of the precipitate in (c,d) with higher magnification where the dark-field image is based on the spot corresponding to the σ-phase marked by an arrow in the SAED pattern in (d), (f) chemical analyses in at.% by EDS for the matrix and precipitate at A and B, respectively.

Fig. 7 SEM observations on longitudinal sections of the CoCrFeNiMn HEA (a) processed by ECAP through four passes at 673 K and after subsequent PDA for 60 min at (b) 873, (c) 973 and (d) 1073 K.

Fig. 8 Stress-strain curves at an initial strain rate of 1.0×10^{-3} s^{-1} after four passes of ECAP processing and with PDA for 60 min at 773, 873 and 973 K.

Fig. 9 Comparison between the calculated and experimental yield stress of samples after ECAP and after ECAP + PDA for 60 min at 773, 873 and 973 K. The contributions from the intrinsic

strength (σ_0), grain boundary strengthening (σ_{gb}), dislocation strengthening (σ_ρ) and precipitation strengthening (σ_P) were calculated using Eqs. (2-4) and the total strengthening was obtained from a simple summation using Eq. (1).

Figure(s)

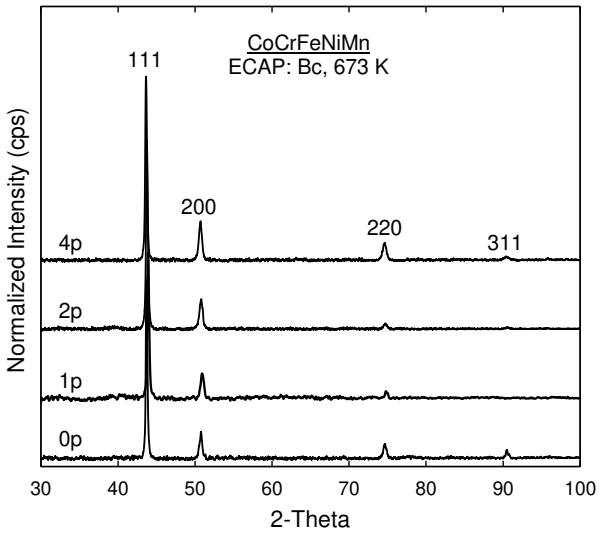

Fig. 1 X-ray patterns of the homogenized (0p) condition and samples processed through one to four passes of ECAP.

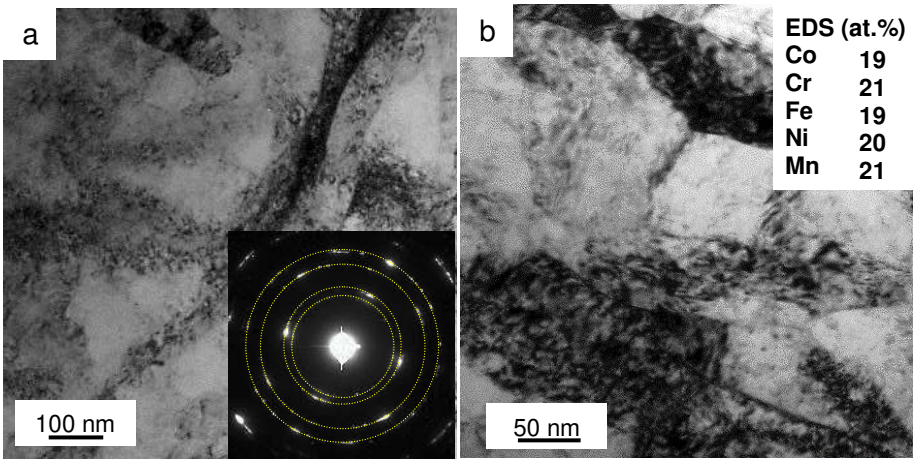

Fig. 2 (a) TEM image and corresponding SAED pattern of transverse section of a CoCrFeNiMn billet processed by ECAP through four passes at 673 K and (b) TEM image with higher magnification and chemical composition after EDS analysis.

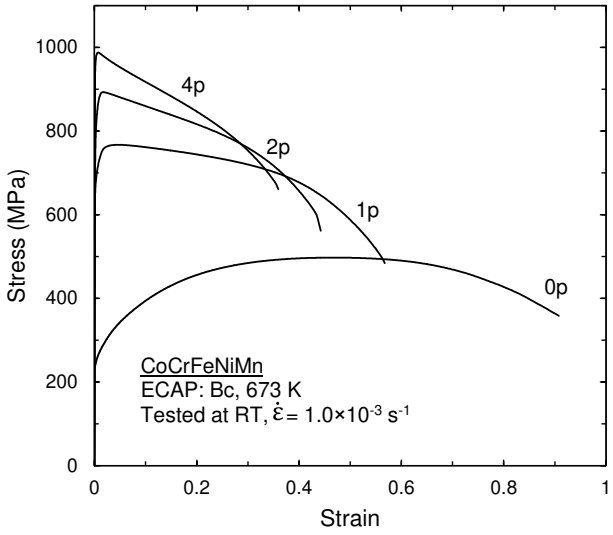

Fig. 3 Stress-strain curves at an initial strain rate of 1.0×10^{-3} s^{-1} in the initial annealed condition (0p) and after ECAP processing through one to four passes.

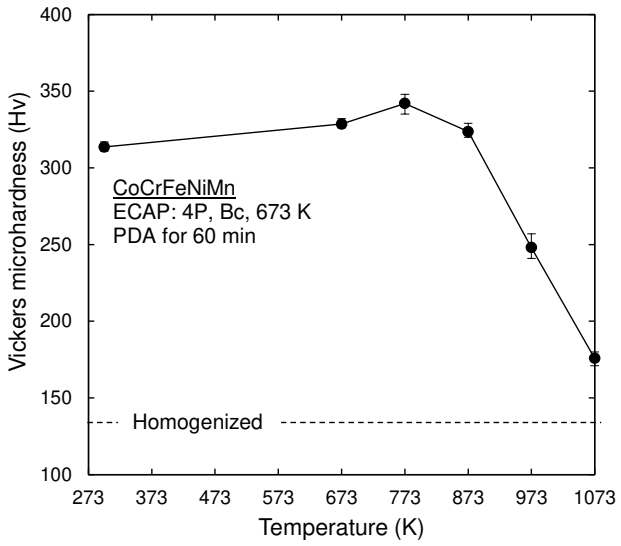

Fig. 4 Dependence of Vickers hardness of the ECAP-processed samples on the annealing temperature when annealing for 60 min: the lower dashed line shows the homogenized initial condition.

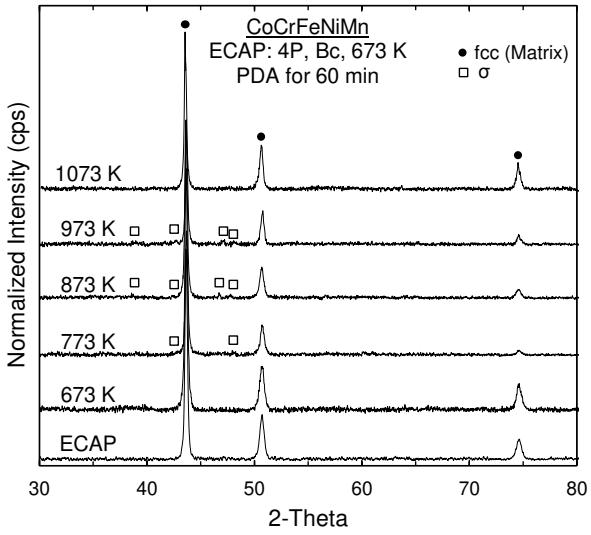

Fig. 5 X-ray patterns after four passes of ECAP followed by PDA at 673 to 1073 K for 60 min.

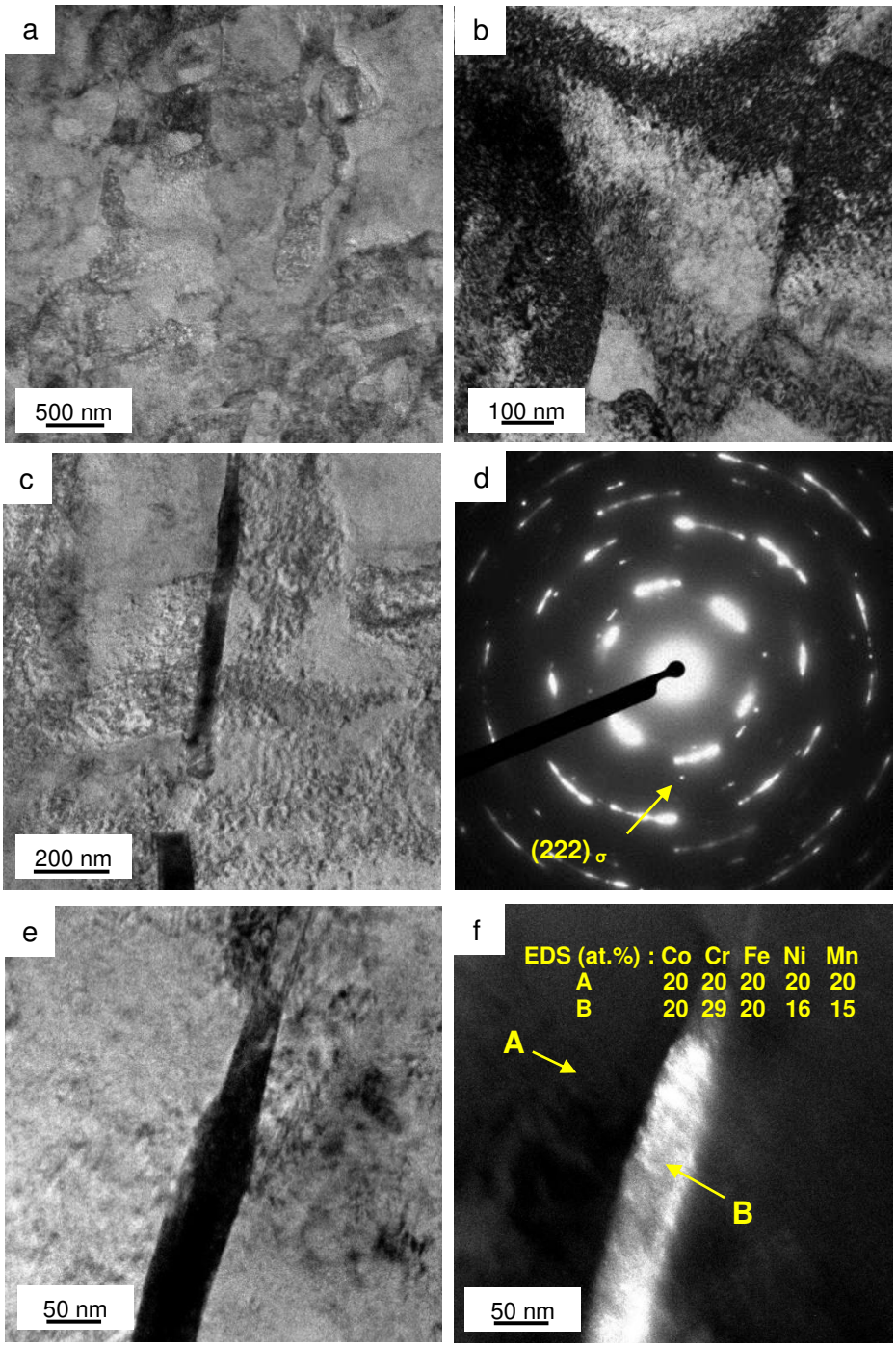

Fig. 6 TEM images of transverse sections of a CoCrFeNiMn HEA processed by ECAP through four passes at 673 K followed by PDA at 773 K for 60 min: (a-c) grains with mean grain size of ~500 nm, (d) corresponding SAED pattern from the area in (c) containing precipitates, (e) bright and (f) dark-field TEM images of the precipitate in (c,d) with higher magnification where the dark-field image is based on the spot corresponding to the σ-phase marked by an arrow in the SAED pattern in (d), (f) chemical analyses in at.% by EDS for the matrix and precipitate at A and B, respectively.

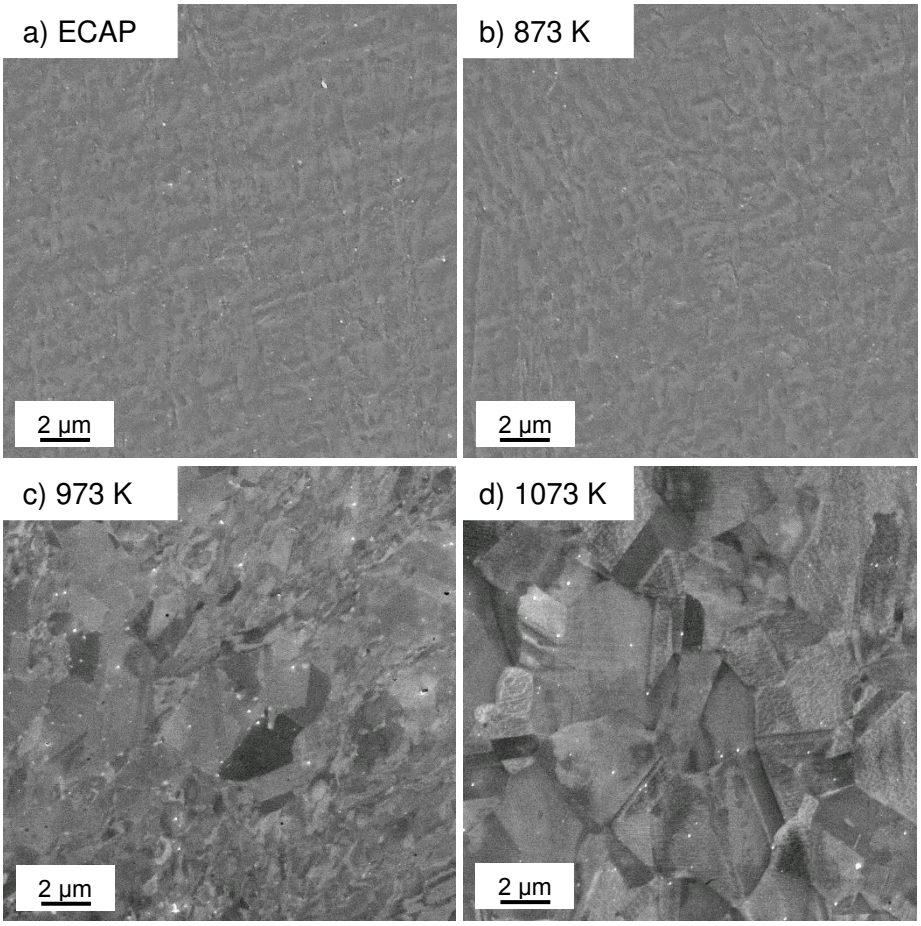

Fig. 7 SEM observations on longitudinal sections of the CoCrFeNiMn HEA (a) processed by ECAP through four passes at 673 K and after subsequent PDA for 60 min at (b) 873, (c) 973 and (d) 1073 K.

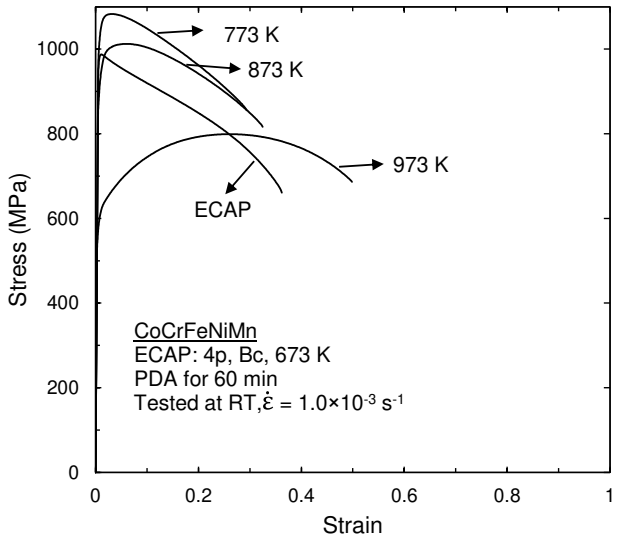

Fig. 8 Stress-strain curves at an initial strain rate of 1.0×10^{-3} s^{-1} after four passes of ECAP processing and with PDA for 60 min at 773, 873 and 973 K.

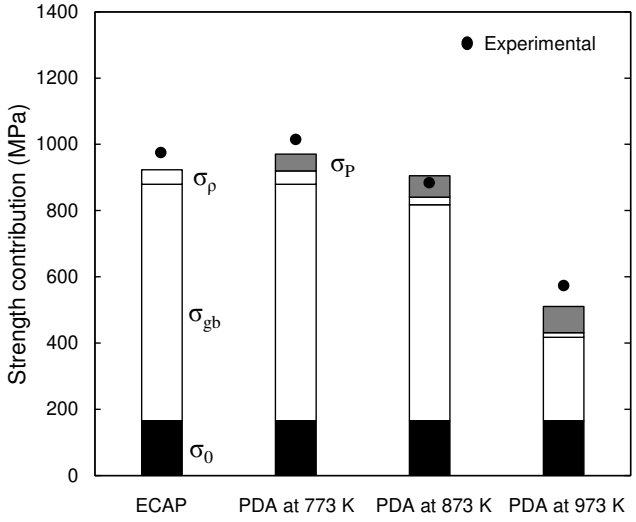

Fig. 9 Comparison between the calculated and experimentally obtained yield stress of ECAP-processed sample and samples after PDA at 773, 873 and 973 K for 60 min. Contributions from intrinsic strength (σ_0), grain boundary strengthening (σ_{gb}), dislocation strengthening (σ_ρ) and precipitation strengthening (σ_P) were calculated using Eqs. (3-4), and simple sum of strengthening contribution obtained based on Eq. (1).

Table(s)

Table 1. The grain size , d, dislocation density , ρ, Vickers microhardness, YS, UTS, elongation to failure (δ) and uniform strain, of the CoCrFeNiMn HEA before and after ECAP processing at 673 K through different numbers of passes.

Number of passes	d (μm)	ρ (cm^{-2})	Hv	YS (MPA)	UTS (MPa)	δ (%)	Uniform strain (%)
0	100	-	135±4	240	500	90	47
1	0.160	3.5×10^{8}	260±8	670	770	55	5
2	0.130	8.1×10^{8}	285±3	810	890	45	2
4	0.100	1.3×10^{9}	315±3	980	990	35	1

Table 2. The Vickers microhardness, YS, UTS, elongation to failure (δ) and uniform strain, of CoCrFeNiMn HEA before and after post-deformation annealing.

Number of passes	Annealing Temp. (K)	Hv	YS (MPA)	UTS (MPa)	δ (%)	Uniform strain (%)
2	-	285±3	810	890	45	2
	773	315±8	850	960	37	4
	873	305±6	820	880	41	8
	973	240±10	530	750	50	26
4	-	315±3	980	990	35	1
	773	340±6	1015	1080	30	3
	873	320±5	890	1010	32	6
	973	250±8	560	800	50	26

Table 3. The contributions of intrinsic strength (σ_0), grain boundary strengthening (σ_{gb}), dislocation strengthening (σ_ρ) and precipitation strengthening (σ_P) for each condition and comparison between the calculated and experimentally obtained yield stress of the ECAP-processed sample and samples after PDA at 773, 873 and 973 K for 60 min.

Condition	σ_0 (MPa)	σ_{gb} (MPa)	σ_ρ (MPa)	σ_P (MPA)	$\sigma_{0.2cal}$ (MPA)	$\sigma_{0.2exp}$ (MPA)
ECAP	165	715	44	0	925	985
PDA at 773 K	165	715	40	51	970	1020
PDA at 873 K	165	650	23	65	905	900
PDA at 973 K	165	250	14	79	510	575